ASEAN Journal for Science and Engineering in Materials

Journal homepage: https://ejournal.bumipublikasinusantara.id/index.php/ajsem

Experimental and Bibliometric Analysis of Truncated Cone Fouling Suppression Device for Vortex-Induced Vibration Control in Marine Structures

Noor Idora Mohd Sukarnoor[1], Wan Mohd Norsani Wan Nik[2], Ahmad Hussain[3], Lee Kee Quen[4], Nur Najahatul Huda Saris[4], Suriani Mat Jusoh[2], Fakhratul Ridwan Zulkifli[2]*

[1] Universiti Utara Malaysia, Kedah, Malaysia
[2] Universiti Malaysia Terengganu, Terengganu, Malaysia
[3] DHA Suffa University, Karachi, Pakistan
[4] Universiti Teknologi Malaysia, Johor Bahru, Malaysia
*Correspondence: E-mail: niksani@umt.edu.my

ABSTRACT

Vortex-induced vibration (VIV) poses a critical threat to the integrity and fatigue life of marine and offshore structures. This study evaluates the effectiveness of a truncated cone fouling suppression device in reducing VIV of a low-mass ratio circular cylinder. Experiments were performed in a circulating water flume at Reynolds numbers ranging from 8,000 to 45,000, using various surface coverage ratios. The vibration amplitude and frequency responses were analyzed to determine suppression performance. Results showed that the device reduced oscillation amplitude by up to 68% within the lock-in region, with optimal suppression observed at 25-50% coverage. This indicates that partial surface modification enhances flow–structure interaction and weakens wake coherence. Furthermore, a bibliometric analysis was integrated to identify research trends and gaps in passive vibration control. The present approach provides both scientific and practical insights for developing low-drag, efficient, and sustainable VIV mitigation strategies in marine engineering.

ARTICLE INFO

Article History:
Submitted/Received 04 Aug 2025
First Revised 28 Sep 2025
Accepted 02 Nov 2025
First Available online 03 Nov 2025
Publication Date 01 Sep 2026

Keyword:
Oscillation amplitude,
Passive device,
Truncated cone shape,
Vortex-induced vibration.

1. INTRODUCTION

Vortex-induced vibration (VIV) has been widely studied for decades because of its significant effect on the structural integrity and fatigue life of cylindrical structures such as marine risers, pipelines, and bridge cables (Khalak & Williamson, 1999; Park *et al*., 2015; Yong *et al*., 2025). When a bluff body is subjected to fluid flow, alternating vortices are shed from its surface, creating fluctuating lift forces that generate self-excited oscillations in the transverse direction (Khalak & Williamson, 1999; Shaharuddin & Darus, 2015). As a self-regulating and self-excited phenomenon, VIV can cause severe fatigue damage, increase dynamic loads, and lead to structural instability when oscillations persist for long durations (Lu *et al*., 2023; Cicolin & Assi, 2017). Consequently, the fatigue life of marine risers can be significantly reduced, resulting in safety risks and high maintenance and inspection costs (Yong *et al*., 2025).

Controlling vibration is therefore a critical aspect in the design of marine structures. Numerous studies have proposed both active and passive control techniques to minimize vibration amplitude and extend structural lifespan (Zhao, 2023; Rabiee & Esmaeili, 2020; Liao *et al*., 2023; Korkischko & Meneghini, 2010; Song *et al*., 2021; Sukarnoor *et al*., 2021; Ramzi *et al*., 2022). Among these techniques, passive control devices are particularly attractive because of their simplicity, reliability, and low operational cost. Such devices typically function by modifying surface geometry or introducing three-dimensional disturbances that alter flow separation and vortex shedding patterns (Ran *et al*., 2023; Jiménez-González & Huera-Huarte, 2018; Law & Jaiman, 2018; Bearman & Branković, 2003). Several passive devices, including helical strakes, fairings, splitter plates, and shrouds, have been developed and proven effective in mitigating VIV (Yong *et al*., 2025; Li *et al*., 2025; Sun *et al*., 2020). Helical strakes, for example, can reduce VIV amplitude by up to 70–90%, although they tend to increase drag significantly in water applications (Gao *et al*., 2014; Quen *et al*., 2014; Li *et al*., 2020; Wang *et al*., 2024). Fairings, while effective in both vibration and drag reduction, may experience hydroelastic instability at high flow velocities (Cicolin & Assi, 2017; Park *et al*., 2015).

Beyond these conventional approaches, researchers have also examined the role of surface roughness and geometric modifications in controlling flow separation and vortex shedding. Changes in surface texture affect boundary-layer development, wake structure, and the synchronization between vortex shedding and cylinder motion. Increasing surface roughness delays or disrupts synchronization, thereby reducing vibration amplitude and narrowing the lock-in range (Gao *et al*., 2018). Adding folds or bumps to cylindrical surfaces can enhance turbulence and dissipate energy more effectively, resulting in improved suppression performance, with efficiency increasing as roughness height becomes greater (Wang *et al*., 2021). Biological modifications have also been shown to alter hydrodynamic characteristics. Experiments demonstrated that partial surface coverage by natural elements such as moss can lower vibration amplitude by disturbing wake formation and weakening alternate vortex shedding (Zhu *et al*., 2024).

Marine fouling, which refers to the accumulation of organisms such as barnacles, algae, and hydroids on submerged surfaces, naturally changes the flow regime around marine structures (Gomez-Banderas, 2022; Idora *et al*., 2015). This process modifies surface roughness and alters flow separation points, affecting the formation and synchronization of vortices that cause VIV. The suppression effectiveness of fouling depends on several factors, including the coverage ratio, spatial distribution, and type of fouling, with soft fouling often providing greater damping and vibration reduction (Harandi *et al*., 2024). In addition, bio-inspired surface protrusions and roughness patterns can influence vortex dynamics,

promoting wake instability and thereby reducing VIV amplitude (Zou *et al*., 2024; Wu *et al*., 2024).

An experimental investigation on the influence of marine fouling coverage and morphology on VIV behavior revealed that fouling coverage effectively reduces peak oscillation amplitude, lock-in range, and maximum lift coefficient, while fouling shape alters response branches and synchronization limits. The study further showed that suppression efficiency depends on parameters such as coverage ratio, aggregation, flow incidence, and fouling morphology. These findings demonstrate that the impact of marine fouling on VIV is complex and multidimensional, with both the extent and nature of fouling playing crucial roles in modifying flow–structure interactions. However, the underlying mechanisms through which fouling alters VIV response remain inadequately understood, indicating the need for further systematic analysis.

This study offers a systematic experimental investigation on the influence of truncated cone surface modification as a fouling suppression device for vortex-induced vibration (VIV) control. We also added bibliometric analysis to support this study. Unlike previous works that focused on conventional passive devices such as helical strakes and fairings, this research examines a wider range of coverage ratios under low mass-damping conditions to determine the optimal configuration for vibration suppression. The findings establish a new understanding of how partial surface modification alters wake dynamics, reduces vortex coherence, and improves flow–structure interaction. This contribution provides practical and quantitative insight for developing low-drag, simple, and efficient passive control solutions in marine and offshore structural design.

2. METHODS

2.1. Experimental set-up

The experiments were conducted in a circulating water flume at the National Water Research Institute of Malaysia, which measured 1.5 m in width and 2.0 m in depth. Water flow velocity, generated by a pump, varied from 0.11 to 0.58 m/s, with average increments of 0.02 m/s. Based on the cylinder's diameter and flow velocity, this gave a Reynolds number range of 8,237 to 43,431. Turbulence intensity was measured at 1.9% at an inflow velocity of 0.3 m/s.

A hollow polyvinyl chloride (PVC) cylinder model was used as a model in this experiment. **Figure 1(a)** is the model that we created. The bare cylinder model, vertically mounted (**Figure 1b**) in the test section, had a submerged length (L) of 440 mm and a diameter (D) of 60 mm. Depending on the diameter of the cylinder, the resulting aspect ratio is 6.67-7.33. The cylinder mass ratio (m^*) is 2.97, determined using the formula of $4m/\pi\rho D^2L$, where m is the total mass of a cylinder and ρ is the fluid density. **Figure 2** shows a free decay test, which determined the structural damping coefficient in air to be 0.033, yielding a mass-damping parameter ($m^*\zeta$) of 0.09801. On the other hand, the natural frequency of each cylinder with a truncated cone in water varied from 0.933 to 0.983 Hz, which was obtained from a free decay test. The main properties of the rigid cylinder model are listed in **Table 1**.

Supporting frames secured the test rig, PVC pipe, and sensor to the water flume wall. This system was adapted from the previous design. Two parallel leaf springs (310 mm x 90 mm x 0.95 mm) provided a lateral stiffness of approximately 250 N/m, enabling the cylinder to vibrate in the cross-flow (CF) direction. An accelerometer, positioned near the cylinder and below the leaf springs, recorded the model's amplitude response. The sensor was calibrated before each series of tests. Data was acquired at a rate of 200 Hz.

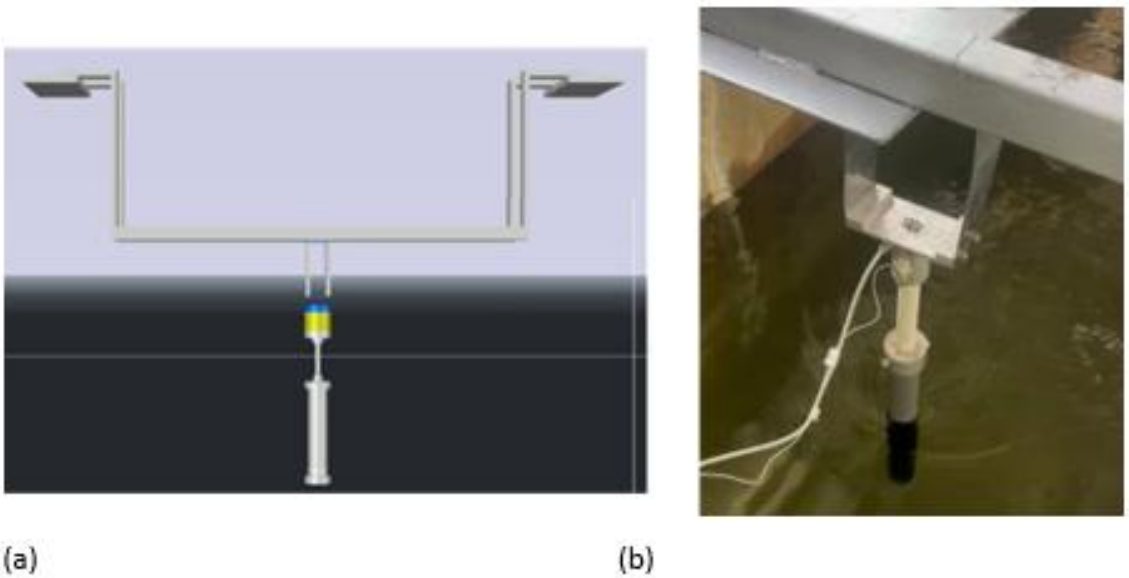

(a) (b)

Figure 1. Experimental setup in the water flume: (a) design; (b) realistic equipment

Table 1. Properties of cylinder model.

	Unit	M1	M2	M3	M4	M5
Coverage ratio	%	0	25	50	75	100
Total Barnacle (*N*)	-		397	794	1190	1568
Mean height of artificial barnacle (h)	mm	0	3	3	3	3
Upper diameter of artificial barnacle (d)	mm	0	3	3	3	3
Relative roughness (ε)	-	0	0.045	0.045	0.045	0.045
Spring stiffness (k)	N/m	250	250	250	250	250
Submerged length of PVC pipe (L)	mm	440	440	440	440	440
Diameter of PVC pipe (D)	mm	60	66	66	66	66
Aspect ratio (L/D)	-	7.33	6.67	6.67	6.67	6.67
Total mass of the cylinder	kg	3.69	3.7	3.71	3.72	3.74
Mass ratio	-	2.97	2.46	2.46	2.47	2.48
Damping in air	-	0.033	0.033	0.033	0.033	0.033
Mass-damping	-	0.09801	0.08118	0.08118	0.08151	0.08184
Reduced velocity	-			1.96-10.36		
Reynolds number	-			8237-43431		

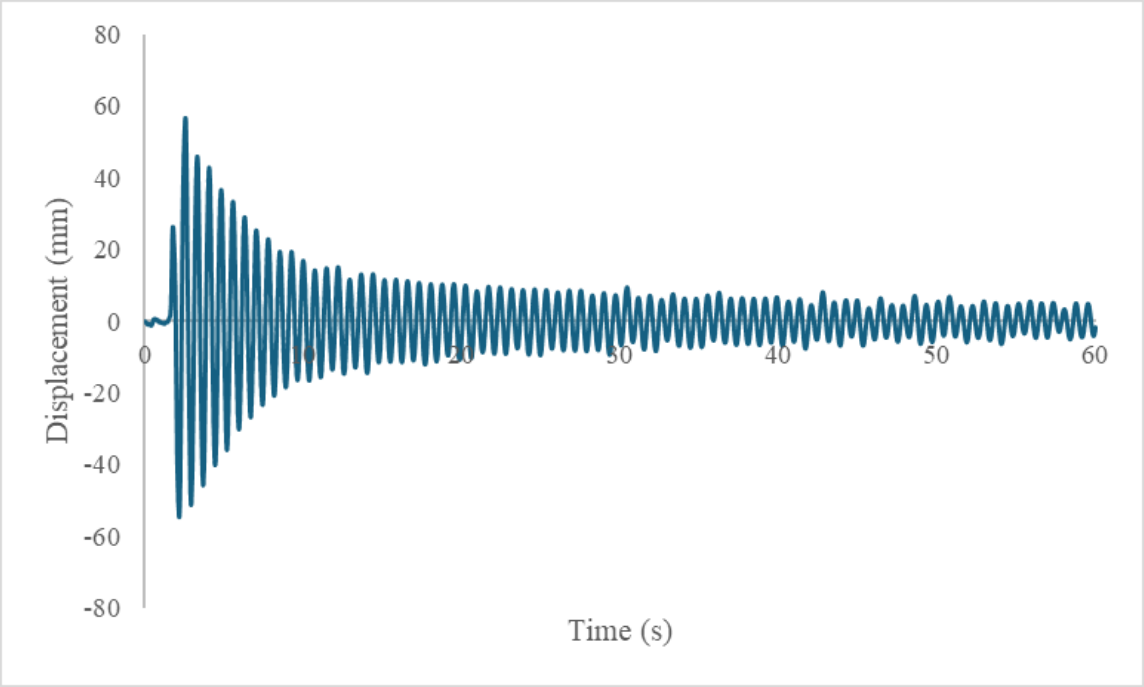

Figure 2. Time series of amplitude response during free decay test.

2.2. Artificial Fouling as a Suppression Device

The fouling shape of truncated cones and semi-spherical protrusions can reduce VIV by disrupting the span-wise correlation and synchronization of vortices shed from the cylinder, thereby reducing the wake size. In designing the artificial fouling, the height and diameter of the truncated cone are key parameters. In this study, the truncated cones were made from Thermoplastic Polyurethane (TPU), an ideal material for submerged applications. A total of two similar fouled sheets (Upper and Lower sheet) were used to cover the submerged length of 440 mm, with a surface area of 82940 mm^2.

2.2.1. Random cluster of truncated cones using Poisson Cluster Process

The distribution of artificial fouling on the cylinder model followed guidelines, utilizing a Poisson Cluster Process (PCP) to generate random clusters of points. This statistical method was employed to accurately model the aggregated spatial distribution of artificial marine fouling, thereby better mimicking natural biofouling settlement patterns. Unlike regular patterns, the PCP generates clumped random distributions, which more closely simulate natural colonization. PCP is based on Equation (1), where Φ is the total point field (truncated cone locations), x is the series of points, Φ_p is the parent Poisson process and n^x is the point of children around the parent.

$$\Phi = \bigcup_{x \in \Phi_p} n^x \tag{1}$$

The total number of barnacles (N) for each coverage ratio of 25, 50, and 75%, which are 397, 794, and 1190, respectively, was predefined based on the ratio of barnacle coverage area to the total unwrapped cylindrical area. **Figure 3** shows the result from the Poisson Cluster Process for 25, 50, and 75%, which are presented in **Figures 3(a), 3(b), and 3(c)**, respectively.

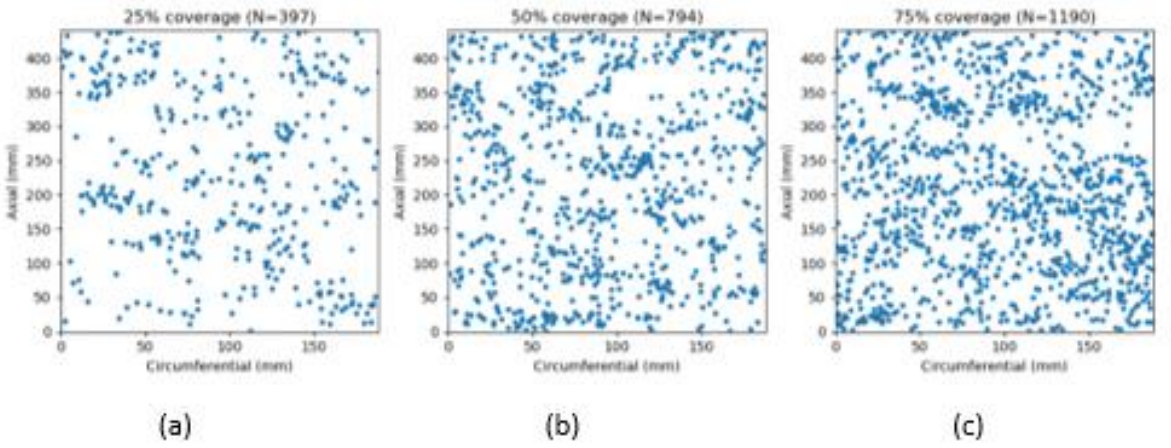

Figure 3. Poisson Cluster Process for truncated cone at a coverage ratio: (a) 25%, (b) 50%, and (c) 75%.

2.2.2. Statistical Verification Using Distance to Nearest Neighbor

To verify the spatial characteristics of the PCP-generated truncated cone distribution, the Distance to Nearest Neighbor (DNN) analysis (Edmonds *et al*., 2015; Clark & Evans, 1954) was used. The DNN index is defined in Equation (2):

$$R = \frac{\bar{r}_A}{\bar{r}_E} \tag{2}$$

where, $\bar{r}_A$ is the mean of the actual nearest neighbor distances measured from each truncated cone center, $\bar{r}_E$ is the expected mean nearest-neighbor distance for a completely random (Poisson) distribution, given by Equation (3):

$$\bar{r}_E = \frac{1}{2\sqrt{\rho}} \tag{3}$$

where $\rho = \frac{N}{A_S}$ represents the spatial density of a truncated cone per unit surface area.

From the DNN analysis, the Clark–Evans *R* index from PCP indicates that the distribution of the truncated cone is clustered, with a value *R* = 0.953 (less than 1). The mean nearest-neighbor distance, $\bar{r}_A$ and the expected random distance, $\bar{r}_E$ values were found to be 3.98 and 4.17 mm, respectively. An *R* value less than one signifies a clustered distribution, whereas values equal and greater than one represent random and regular distributions, respectively (Clark & Evans, 1954). Therefore, the generated pattern confirms that the truncated-cone elements exhibit non-random, clustered spatial characteristics. This observation is consistent with the previous findings, who reported a similar clustered pattern with *R* ≈ 0.88.

Figure 4 illustrates the coverage ratio of the upper sheet of artificial fouling, with 100% designated as a regular distribution with N = 1568. We showed the coverage ratios of 25, 50, 75, and 100%, corresponding to **Figures 4(a), 4(b), 4(c), and 4(d)**. The artificial marine fouling was modeled as truncated cones with a mean height of 3 mm, representing an approximate 30-mm height in real conditions, and the larger diameter was set to be twice the smaller diameter.

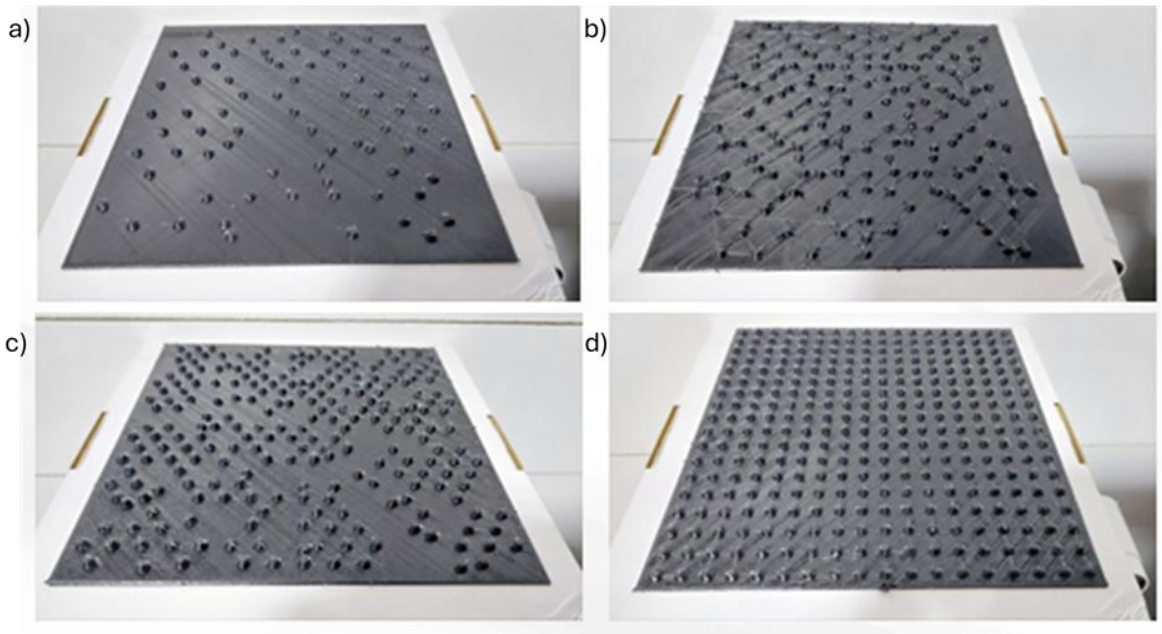

Figure 4. Artificial fouling of truncated cone on upper sheet, with coverage ratio: (a) 25%, (b) 50%, (c) 75%, and (d) 100%.

3. RESULTS AND DISCUSSION

3.1. Bibliometric Analysis

A bibliometric analysis using the Scopus database revealed a rapid and consistent increase in research related to marine studies, totaling 666,696 indexed documents from 1867 to 2025 (**Figure 5**). Publication growth accelerated sharply after 2010, indicating the global expansion of multidisciplinary research in marine engineering, ocean sustainability, and offshore technologies. In 2025 alone, 37,246 documents were published, reflecting sustained scientific attention to marine-related innovation. This upward trend underscores the growing importance of hydrodynamic stability, energy-efficient design, and vibration control within marine applications, positioning the present study within a highly active and evolving research domain.

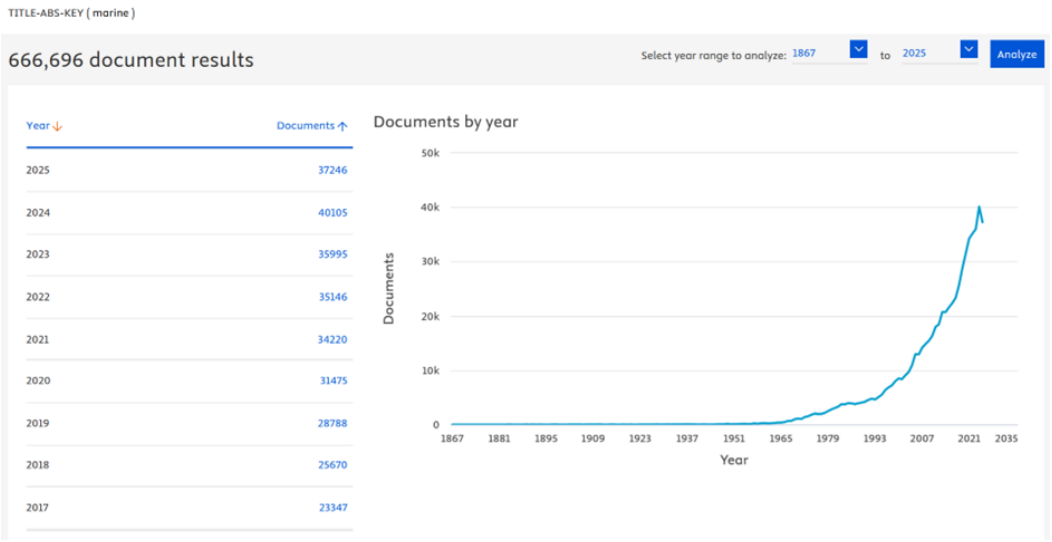

Figure 5. Bibliometric analysis from Scopus database using keyword “marine”, taken on November 2025.

3.2. Validation of the Study

The VIV experiment in this present study is validated by comparing its amplitude response with previous data. **Figure 6** shows the graph of maximum CF amplitude ratio (A_y/D) versus reduced velocity (U_r) obtained through an equation of U/f_nD, where U is the velocity of the water, f_n is the natural frequency, and D is the diameter of the cylinder. The amplitude response pattern of the bare cylinder in this study demonstrates good agreement with the previous findings. No significant vibration response was observed in the reduced velocity range of $2.0 < U_r < 3.9$. The cylinder began to vibrate at $3.93 < U_r < 9.28$, maintaining consistent oscillations beyond U_r = 9.646. This observation aligns with previous studies, where a remarkable feature was the absence of a lower branch in their amplitude response, showing no indication of decreasing even near U_r = 10. Due to limitations of the experimental water flume in this study, it was not possible to increase water speed sufficiently to completely observe the lower branch of the amplitude response. This absence of a lower branch at $U_r >$ 6 is likely attributable to the smaller mass ratios (m^* = 4) in their experiment. Indeed, this contrasts with previous works where the lower branch was observed in systems with larger mass ratios. This perspective is further supported by references (Assi *et al*., 2009; Assi *et al*., 2010), indicating that smaller mass ratio systems (m^* = 2.0) may show no differences between initial and upper branches, with the lower branch appearing much later, around $U_r \geq 10$, thereby confirming the significant impact of mass ratio on VIV characteristics.

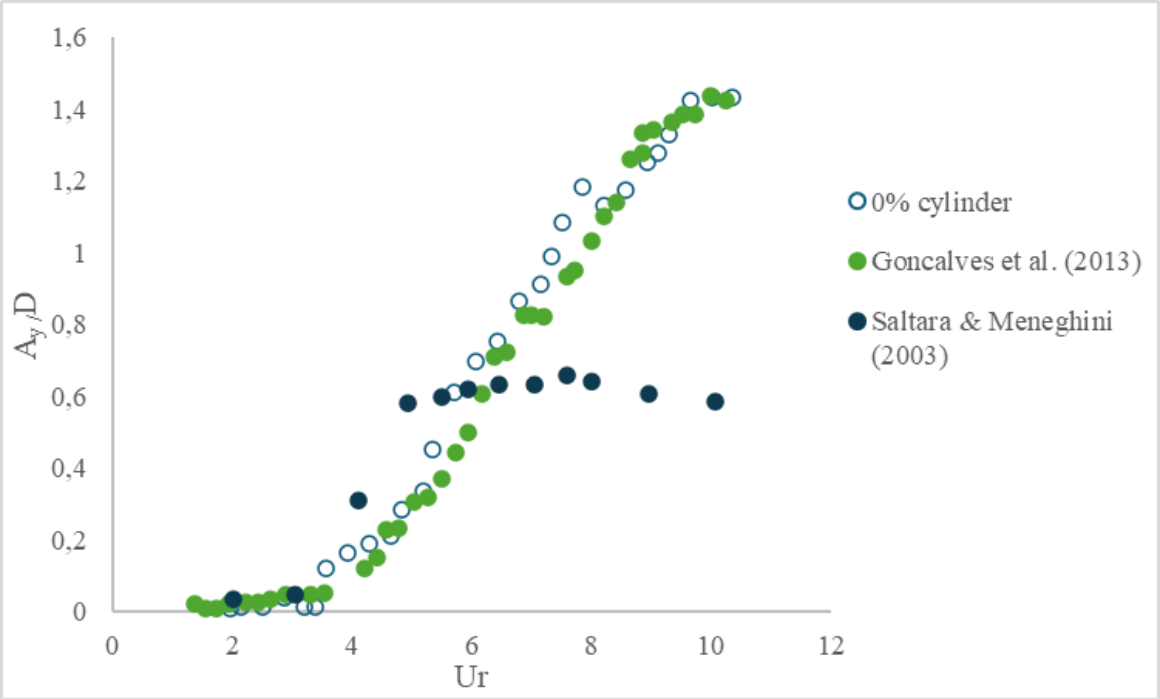

Figure 6. Result of the amplitude ratio for the bare cylinder from the present and previous studies.

3.3. Effect of Truncated-Cones on Vibration Amplitude

Figure 7 illustrates the influence of artificial fouling, at coverage ratios of 0, 25, 50, 75, and 100%, on the cylinder's vibration amplitude response, providing insights into the performance of truncated cones in suppressing VIV. A notable observation from the amplitude response is the significant reduction in the peak amplitude of fouled cylinders compared to the bare cylinder across the range of tested reduced velocities. Initially, for all fouled configurations, the amplitude increased steadily, remaining below an amplitude ratio, A_y/D = 0.3, suggesting

a general suppressive effect of the truncated cones. However, distinct behavioral differences emerged at higher reduced velocities, where the oscillation amplitude for cylinders with 25 and 50% coverage ratios decreased, reaching a minimum amplitude ratio of approximately 0.17*D*. In contrast, the cylinders with 75 and 100% coverage ratios exhibited a continuous increase in amplitude at higher reduced velocities, approximately 0.37*D*. The highest amplitude ratio for a fouled cylinder was observed at U_r = 10.03 for the cylinder with a 100% coverage ratio. This critical observation indicates that less dense coverage ratios of truncated cones are more effective in suppressing vibration. These findings align with previous research, which similarly found that a cylinder with a 100% coverage ratio exhibited less suppression efficiency compared to configurations with smaller coverage ratios, such as 33%. Interestingly, the suppression efficiency emphasizes that higher coverage does not invariably lead to improved suppression. The introduction of a truncated cone passive device on the cylinder promotes three-dimensional wake disturbances, creates sufficient disturbance to disrupt existing vortices while simultaneously leaving enough gaps to hinder the formation of a new large-scale wake, thus reducing amplitude and altering wake structure (Bearman & Branković, 2004).

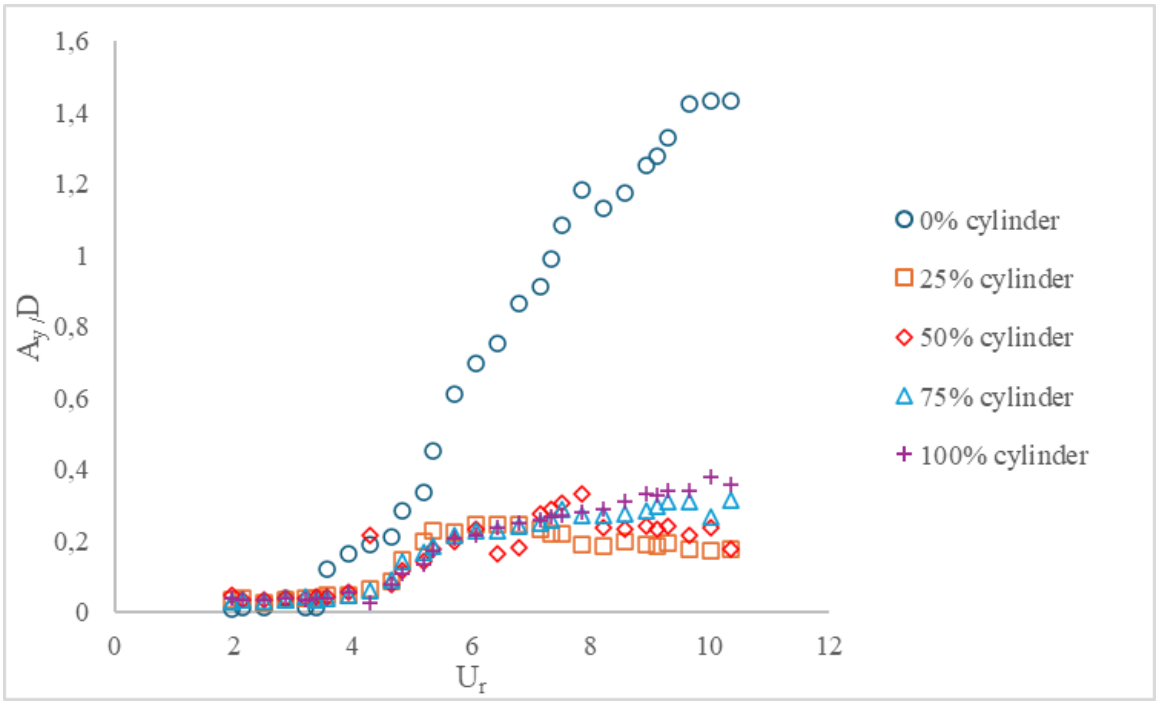

Figure 7. Amplitude response of truncated cone with different coverage ratios

3.4. Effect of Vibration Frequency

Figure 8 compares the frequency responses of the bare cylinder and fouled cylinders with coverage ratios of 25, 50, 75, and 100%. The time series of amplitude responses was converted using Fast Fourier Transform (FFT) to obtain the frequency response. Typically, for smooth circular cylinders in the subcritical Reynolds number range ($10^3 < Re < 10^5$), the Strouhal number (*St*) is approximately 0.2 (Modir & Goudarzi, 2018). However, the analysis of the frequency response in this present study revealed a Strouhal number of 0.1125, which is notably smaller than this conventional value.

Research indicates that the *St* value is highly sensitive to aspect ratios below 13, with values consistently lower than those observed for high aspect ratio cylinders. St number of 0.111 for

an L/D = 7.5 cylinder, consistent with the present findings. This reduction is primarily due to the formation of a three-dimensional wake (Cicolin & Assi, 2017; Rahman & Thiagarajan, 2015a), which induces a more turbulent region and consequently leads to a decreased frequency of vortex shedding.

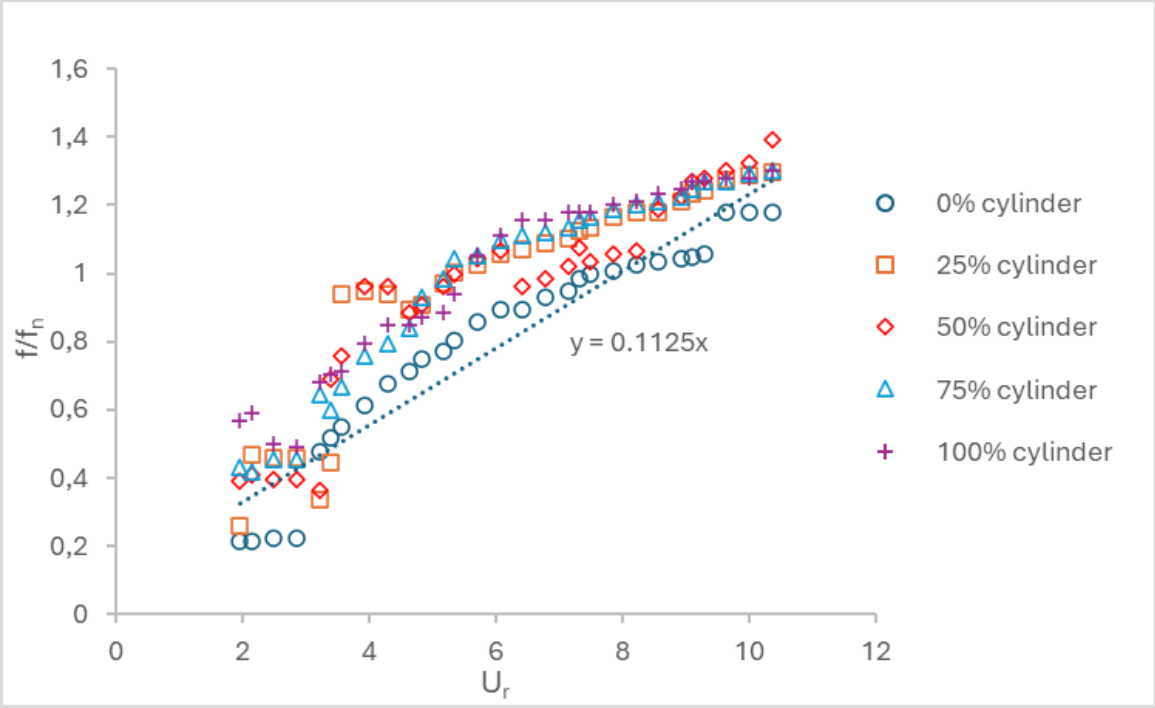

Figure 8. Frequency response of a bare and fouled cylinder.

The cylinders fitted with truncated cones began to vibrate at a reduced velocity of U_r = 4.28, and the vibration amplitude increased with further increments in flow velocity. Notably, the frequency ratio (ratio of response frequency to natural frequency) approached unity beyond U_r = 5.35, signifying the onset of the lock-in phenomenon for all coverage ratios. The phenomenon of "synchronization" or "lock-in" is observed when the frequency of vortex shedding aligns with or approaches the natural frequency of the cylinder, leading to a significant increase in vibration amplitudes (Modir & Goudarzi, 2018; Park *et al.*, 2015). However, the frequency response pattern in **Figure 8** reveals a non-classical lock-in behavior rather than a classical three-branch response. This behavior is attributed to the low mass ratio of the system (m* = 2.46–2.97), in which the structure's response frequency is not strictly locked to the vortex-shedding frequency throughout the lock-in range. Instead, the synchronization occurs gradually, and the amplitude exhibits a single continuous branch without a distinct lower branch. The absence of a lower branch and the extended synchronization range confirm that the system follows the characteristics of non-classical lock-in, typically observed in light, low-damping cylinders (Gonçalves *et al.*, 2013; Assi *et al.*, 2010).

4. CONCLUSION

This study examined the efficacy of truncated cones in mitigating VIV on a circular cylinder. In a low-mass system, coverage ratios as low as 25–50% were able to suppress peak amplitudes by up to ~68% compared to a bare cylinder. The findings indicate that specific coverage ratios effectively reduce amplitude response and modify frequency characteristics. Notably, configurations with lower coverage ratios, such as 25%, exhibited superior VIV

suppression compared to those with higher coverage ratios, including 100%. This suggests that an optimal balance between surface modification and flow interaction is crucial for effective VIV suppression, rather than simply maximizing the modified surface area. Future research should explore the behavior of these suppression mechanisms, particularly under higher reduced velocity, to have a deep understanding of the amplitude response under varying mass-damping parameters.

This study examined the effectiveness of a truncated cone fouling suppression device in mitigating VIV of a circular cylinder under low mass-damping conditions. Experimental results demonstrated that coverage ratios of 25–50% significantly reduced vibration amplitude, achieving up to 68% suppression within the lock-in region. The findings indicate that partial surface modification enhances flow–structure interaction and disrupts vortex synchronization more effectively than full coverage. This confirms that an optimal balance between surface modification and flow disturbance is essential for efficient VIV suppression. In addition, a brief bibliometric analysis further revealed increasing global research interest in this study. These insights reinforce the scientific relevance and applicability of the present findings in advancing low-drag, energy-efficient design strategies for marine and offshore structures.

5. ACKNOWLEDGMENT

We would like to thank Universiti Malaysia Terengganu, Malaysia, for providing funding support for this study (UMT/TAPE-RG/2023/55468).

6. AUTHORS' NOTE

The authors declare that there is no conflict of interest regarding the publication of this article. Authors confirmed that the paper was free of plagiarism.

7. REFERENCES

Assi, G. R. S., Bearman, P. W., and Kitney, N. (2009). Low drag solutions for suppressing vortex-induced vibration of circular cylinders. *Journal of Fluids and Structures, 25*, 666–675.

Assi, G. R. S., Bearman, P. W., Kitney, N., and Tognarelli, M. A. (2010). Suppression of wake-induced vibration of tandem cylinders with free-to-rotate control plates. *Journal of Fluids and Structures, 26*, 1045–1057.

Bearman, P., and Branković, M. (2003). Experimental studies of passive control of vortex-induced vibration. *European Journal of Mechanics - B/Fluids, 23*(1), 9–26.

Cicolin, M. M., and Assi, G. R. S. (2017). Experiments with flexible shrouds to reduce the vortex-induced vibration of a cylinder with low mass and damping. *Applied Ocean Research, 65*, 290–301.

Clark, P. J., and Evans, F. C. (1954). Distance to nearest neighbor as a measure of spatial relationships in populations. *Ecology, 35*(4), 445–453.

Edmonds, M., Brett, A., Herd, R. A., Humphreys, M. C. S., and Woods, A. (2015). Magnetite-bubble aggregates at mixing interfaces in andesite magma bodies. *Special Publications, 410*, 7–15.

Gao, Y., Fu, S., Ma, L., and Chen, Y. (2014). Experimental investigation of the response performance of VIV on a flexible riser with helical strakes. *Ships and Offshore Structures, 11*(2), 113–128.

Gao, Y., Zong, Z., Zou, L., and Jiang, Z. (2018). Effect of surface roughness on vortex-induced vibration response of a circular cylinder. *Ships and Offshore Structures, 13*(1), 28–42.

Gomez-Banderas, J. (2022). Marine natural products: A promising source of environmentally friendly antifouling agents for the maritime industries. *Frontiers in Marine Science, 9*, 858757.

Gonçalves, R. T., Rosetti, G. F., Franzini, G. R., Meneghini, J. R., and Fujarra, A. L. C. (2013). Two-degree-of-freedom vortex-induced vibration of circular cylinders with very low aspect ratio and small mass ratio. *Journal of Fluids and Structures, 39*, 237–257.

Harandi, M., Tamimi, V., Zeinoddini, M., Rashki, M., and Ashrafipour, H. (2024). Effects of soft marine growth on vortex-induced vibration: A comparative analysis with hard marine growth. *Applied Ocean Research, 149*, 103906.

Idora, M. N., Ferry, M., Nik, W. W., and Jasnizat, S. (2015). Evaluation of tannin from *Rhizophora apiculata* as natural antifouling agents in epoxy paint for marine application. *Progress in Organic Coatings, 81*, 125–131.

Jiménez-González, J. I., and Huera-Huarte, F. (2018). Vortex-induced vibrations of a circular cylinder with a pair of control rods of varying size. *Journal of Sound and Vibration, 431*, 163–178.

Khalak, A., and Williamson, C. H. K. (1999). Motions, forces and mode transitions in vortex-induced vibrations at low mass-damping. *Journal of Fluids and Structures, 13*, 813–851.

Korkischko, I., and Meneghini, J. R. (2010). Experimental investigation of flow-induced vibration on isolated and tandem circular cylinders fitted with strakes. *Journal of Fluids and Structures, 26*(4), 611–620.

Law, Y., and Jaiman, R. (2018). Passive control of vortex-induced vibration by spanwise grooves. *Journal of Fluids and Structures, 81*, 289–302.

Li, P., Liu, L., Dong, Z., Wang, F., and Guo, H. (2020). Investigation on the spoiler vibration suppression mechanism of discrete helical strakes of deep-sea riser undergoing vortex-induced vibration. *International Journal of Mechanical Sciences, 172*, 105410.

Li, X., Peng, Y. X., Liu, N. N., and Sun, P. N. (2025). Experimental and numerical study on vibration suppression mechanism of vortex induced vibration in riser. *Ocean Engineering, 329*, 121098.

Liao, W., Huang, Z., Sun, H., Huang, X., Gu, Y., Chen, W., Zhang, Z., and Kan, J. (2023). Numerical investigation of cylinder vortex-induced vibration with downstream plate for vibration suppression and energy harvesting. *Energy, 284*, 128264.

Lu, Y., Yu, Z., Liu, Y., and Xu, W. (2023). Fatigue damage characteristics of a flexible cylinder under concomitant excitation of time-varying axial tension and VIV. *Ocean Engineering, 266*, 116079.

Modir, A., and Goudarzi, N. (2018). Experimental investigation of Reynolds number and spring stiffness effects on vortex-induced vibrations of a rigid circular cylinder. *European Journal of Mechanics - B/Fluids, 74*, 34–47.

Park, H., Kumar, R. A., and Bernitsas, M. M. (2015). Suppression of vortex-induced vibrations of rigid circular cylinder on springs by localized surface roughness at $3\times10^4 \leq Re \leq 1.2\times10^5$. *Ocean Engineering, 111*, 218–230.

Quen, L. K., Abu, A., Kato, N., Muhamad, P., Sahekhaini, A., and Abdullah, H. (2014). Investigation on the effectiveness of helical strakes in suppressing VIV of flexible riser. *Applied Ocean Research, 44*, 82–91.

Rabiee, A., and Esmaeili, M. (2020). Simultaneous vortex- and wake-induced vibration suppression of tandem-arranged circular cylinders using active feedback control system. *Journal of Sound and Vibration, 469*, 115131.

Ramzi, N. A. S., Quen, L. K., Senga, H., Kang, H. S., Lim, M. H., and Sukarnoor, N. I. M. (2022). Suppression of vortex-induced vibration of a rigid cylinder using flexible shrouding. *Applied Ocean Research, 123*, 103154.

Ran, Y., Deng, Z., Yu, H., Chen, W., and Gao, D. (2023). Review of passive control of flow past a circular cylinder. *Journal of Visualization, 26*(1), 1–44.

Shaharuddin, N. M. R., and Darus, I. Z. M. (2015). Experimental study of vortex-induced vibrations of flexibly mounted cylinder in circulating water tunnel. *Acta Mechanica, 226*(11), 3795–3808.

Song, J., Chen, W., Guo, S., and Yan, D. (2021). Study on suppressing the vortex-induced vibration of flexible riser in frequency domain. *Applied Ocean Research, 112*, 102882.

Sukarnoor, N., Quen, L., Abu, A., Kuwano, N., Hooi-Siang, K., and Desa, S. (2021). The effectiveness of helical strakes in suppressing vortex-induced vibration of tandem circular cylinders. *Ain Shams Engineering Journal, 12*(5), 467–478.

Sun, X., Suh, C. S., Ye, Z. H., and Yu, B. (2020). Dynamics of a circular cylinder with an attached splitter plate in laminar flow: A transition from vortex-induced vibration to galloping. *Physics of Fluids, 32*(2), 1–14.

Wang, W., Mao, Z., Song, B., and Tian, W. (2021). Suppression of vortex-induced vibration of a cactus-inspired cylinder near a free surface. *Physics of Fluids, 33*(6), 1–12.

Wang, Y., Li, P., Zhang, Y., Liu, Z., Ren, X., Zhu, L., and Dong, S. (2024). Vibration suppression performance evolution process of helical straked riser under coupled interference effect. *Applied Ocean Research, 149*, 104040.

Wu, R., Liu, J., Qu, J., and Guo, A. (2024). Vortex-induced vibration suppression of cactus-like cylinders. *Ocean Engineering, 284*, 117201.

Yong, R., Quen, L. K., Ken, T. L., Yak, X. C., Kang, H. S., and Wong, K. (2025). Experimental investigation on the suppression of vortex-induced vibration of a rigid cylinder using axial slats. *Ocean Engineering, 338*, 121934.

Zhao, M. (2023). A review of recent studies on the control of vortex-induced vibration of circular cylinders. *Ocean Engineering, 285*, 115389.

Zhu, H., Li, Y., Hao, H., Alam, M., Zhou, T., and Tang, T. (2024). Experimental investigation on the vortex-induced vibration of a circular cylinder partially covered with moss. *Ocean Engineering, 285*, 117198.

Zou, J., Zhou, B., Liu, H., Yi, W., Lu, C., and Luo, W. (2024). Numerical study of vortex-excited vibration of flexible cylindrical structures with surface bulge. *Journal of Marine Science and Engineering, 12*(11), 1894.